

Quantum Scars and Regular Eigenstates in a Chaotic Spinor Condensate

Bertrand Evrard^{1,*}, Andrea Pizzi², Simeon I. Mistakidis^{3,2}, and Ceren B. Dag^{3,2,†}

¹*Institute for Quantum Electronics, ETH Zürich, CH-8093 Zürich, Switzerland*

²*Department of Physics, Harvard University, Cambridge, Massachusetts 02138, USA*

³*ITAMP, Center for Astrophysics, Harvard and Smithsonian, Cambridge, Massachusetts 02138, USA*



(Received 24 June 2023; accepted 28 November 2023; published 8 January 2024)

Quantum many-body scars consist of a few low-entropy eigenstates in an otherwise chaotic many-body spectrum, and can weakly break ergodicity resulting in robust oscillatory dynamics. The notion of quantum many-body scars follows the original single-particle scars introduced within the context of quantum billiards, where scarring manifests in the form of a quantum eigenstate concentrating around an underlying classical unstable periodic orbit. A direct connection between these notions remains an outstanding problem. Here, we study a many-body spinor condensate that, owing to its collective interactions, is amenable to the diagnostics of scars. We characterize the system's rich dynamics, spectrum, and phase space, consisting of both regular and chaotic states. The former are low in entropy, violate the eigenstate thermalization hypothesis, and can be traced back to integrable effective Hamiltonians, whereas most of the latter are scarred by the underlying semiclassical unstable periodic orbits, while satisfying the eigenstate thermalization hypothesis. We outline an experimental proposal to probe our theory in trapped spin-1 Bose-Einstein condensates.

DOI: [10.1103/PhysRevLett.132.020401](https://doi.org/10.1103/PhysRevLett.132.020401)

Introduction.—Isolated many-body systems out of equilibrium are typically expected to thermalize, meaning that the expectation value of generic physical observables reaches at long times the value predicted by a thermal ensemble. In this context, thermalization can be understood in terms of the eigenstate thermalization hypothesis (ETH) [1–5], according to which most energy eigenstates are expected to be thermal [6]. However, some systems escape this paradigm with mechanisms such as integrability [7–9], Hilbert space fragmentation [10,11], many-body localization [12–14], and recently quantum many-body scars (QMBS) [15–24]. The latter lead to a weak ergodicity breaking phenomenon [19], whereby a few nonthermal states largely overlap with the initial condition. This results in robust oscillatory dynamics [17], as first experimentally observed in a Rydberg atom array [16].

The notion of quantum scars originates from quantum billiards [25,26]. There, “scars” manifest in the eigenstate wave functions as a higher probability density in the vicinity of unstable periodic orbits (UPO) of the underlying chaotic classical motion [27]. Such an analysis cannot be directly performed on many-body quantum systems lacking a classical limit. Therein, QMBS are usually identified as nonthermal states embedded in the bulk of the energy spectrum [19]. A connection to single-particle quantum scars was suggested for the PXP model in Ref. [28] and further elaborated in Refs. [29,30], relying on variational approaches to construct low-dimensional effective phase spaces. It was found that the periodic revivals associated to QMBS correspond to periodic orbits in the effective phase

space. The region of phase space surrounding these periodic orbits is however regular (i.e., nonchaotic), unlike in scars. To date, the relation of QMBS to scars and regular states thus remains unclear [29].

Here, we address this problem from a fresh perspective, namely that of many-body systems with all-to-all interactions [31–38]. While interacting, these systems have a well-defined classical limit, and thus allow one to unambiguously discern regular and scar states. More specifically, we introduce a chaotic model based on spinor condensates [39,40] which are established experimental platforms to probe quantum many-body physics out of equilibrium [41–45]. We find that the majority of the eigenstates are thermal, featuring close-to-maximal entropy as expected for a chaotic system; see Fig. 1(a). Interestingly, however, most of these thermal states are scarred by a UPO in the underlying classical phase space [Figs. 1(c) and 1(d)], to an extent that we quantify via a scariness figure of merit. This ubiquity of scarring [27,46–48] stands in contrast to the usual phenomenology of QMBS. On the other hand, a smaller fraction of the Hilbert space consists of nonthermal eigenstates, which feature low entanglement entropy, violate ETH, and are as such strongly reminiscent of QMBS. Furthermore, they are organized in “towers” and can be approximately reproduced using a spectrum generating algebra, a generic structure that underlies ergodicity breaking in a variety of situations, for instance in two-dimensional quantum gases [49], in the Hubbard model [50], or in various models hosting QMBS [17–19,22–24]. However, in the mean-field phase space, these nonthermal states

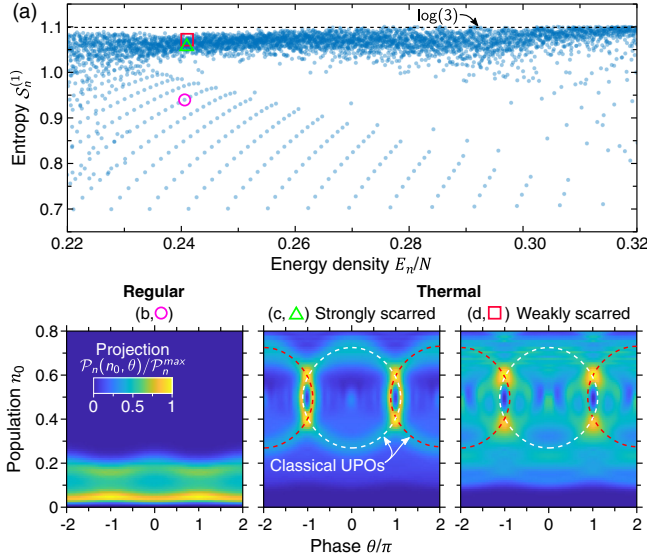


FIG. 1. (a) The entanglement entropy $S_n^{(1)}$ of the eigenvalues of one-body reduced density matrix with respect to energy density E_n/N . $S_n^{(1)}$ distinguishes thermal eigenstates, which nearly saturate the upper bound $S_n^{(1)} = \ln 3 \approx 1.1$, from an array of towers of regular eigenstates with lower entropy. (b)–(d) Phase space distributions $\mathcal{P}_n(n_0, \theta)$ of selected eigenstates, corresponding to the purple circle, green triangle, and red square markers in panel (a). Regular states (b) lie within a restricted region of the phase space, whereas the scarred states (c),(d) concentrate around the classical UPOs (white and red dashed lines) to some variable degree [strong for (c), scariness $D_n \approx 2.1$, and weak for (d), $D_n \approx 1.2$]. Here, we consider $N = 200$ particles.

are associated to stable orbits forming regular regions [Fig. 1(b)]. They are not affected by the UPOs, in contrast to scars as defined in [27] and shown in Figs. 1(c) and 1(d). Thus, in our model, QMBS properties are found in regular states and not in quantum scars.

We conclude by investigating the dynamical signature of regular and scarred eigenstates. While the former give rise to robust oscillatory dynamics and prevent thermalization, the latter does not, but can cause a finite revival of the time-evolved state fidelity before thermalization. Our work sheds light on the fundamental differences between two notions of scars found in the single- and many-body systems [18,19,24,27], and puts spinor condensates forward as a prominent platform for the experimental investigation of scarring.

Model.—We consider N spin-1 bosonic atoms tightly confined in an optical trap, such that spin and spatial degrees of freedom decouple, and condensation occurs in a single spatial orbital [51–56]. This limit is achieved for a strong trapping potential and small atom number [57], such that the kinetic energy sets the largest energy scale, and the cost of a spatial mode excitation is much larger than that of a spin excitation. The low energy physics is therefore governed by a spin Hamiltonian, reading

$$\hat{H}_{\text{spin}} = \frac{c_1}{N} \sum_{i < j} \hat{\mathbf{s}}_i \cdot \hat{\mathbf{s}}_j + \sum_i (p_z \hat{s}_{z,i} + q \hat{s}_{z,i}^2 + \mathbf{p}_\perp(t) \cdot \hat{\mathbf{S}}_{\perp,i}). \quad (1)$$

In Eq. (1), the first term describes an all-to-all Heisenberg interaction with strength c_1/N [39]. In the second sum, the first two terms correspond to the linear ($p_z \propto B_z$) and quadratic ($q \propto B_z^2$) Zeeman energies in the presence of a large static magnetic field B_z along the z axis. The last term is the linear Zeeman energy due to a sum of two weak fields rotating in the (xy) plane at the frequencies $p_z \pm q$, thereby driving the hyperfine transition $0 \leftrightarrow \pm 1$. Performing a change of frame described in the Supplemental Material (SM) [58], we obtain the time-independent Hamiltonian

$$\hat{H} = \frac{c_1}{N} \left[\hat{N}_0(N - \hat{N}_0) + \frac{1}{2} (\hat{N}_+ - \hat{N}_-)^2 \right] + p(\hat{W}_+ + \hat{W}_-), \quad (2)$$

where $\hat{N}_m = \hat{a}_m^\dagger \hat{a}_m$, with \hat{a}_m the annihilation operator for the spin mode $m = 0, \pm 1$, $\hat{W}_\pm = (1/\sqrt{2})(\hat{a}_\pm^\dagger \hat{a}_0 + \text{H.c.})$, and p is the Larmor frequency associated with the rotating transverse field. In the limit $p = 0$ the populations \hat{N}_m are conserved and the model is integrable, whereas a finite p introduces tunneling between different modes m , breaks integrability, and leads to richer dynamics. An interesting feature of the interaction term in Eq. (2) is a logarithmic divergence of the density of states in the middle of the energy spectrum [58]. In contrast to previous studies of chaotic spinor condensates [35,56], this key feature allows for the rapid emergence of quantum chaos, as commonly diagnosed by energy level statistics and entanglement entropy [5], even for $p \ll c_1$. For concreteness, we will focus on $p = 0.05$, near the onset of chaos, and set $c_1 = \hbar = 1$ [69].

To gain insights into the dynamics, we begin by deriving the corresponding semiclassical (mean-field) equations of motion. To this end, we define a $\text{SU}(3)$ coherent state $|\zeta\rangle = (1/\sqrt{N!})[\sum_m \zeta_m \hat{a}_m^\dagger]^N |0\rangle$ with $\zeta_m = \sqrt{n_m} e^{i\phi_m}$, where $n_m \equiv N_m/N$. Enforcing normalization, $\sum_m n_m = 1$, and choosing the global phase such that $\phi_0 = 0$, we can parametrize the coherent states by four real numbers, n_0 , $\theta = \phi_+ + \phi_-$, $m = n_+ - n_-$, and $\eta = \phi_+ - \phi_-$, yielding mean-field equations of motion,

$$\begin{aligned} \dot{n}_0 &= p\sqrt{2n_0}[\sqrt{n_+} \sin \phi_+ + \sqrt{n_-} \sin \phi_-], \\ \dot{\theta} &= 2(1 - 2n_0) + p \left[\frac{2n_+ - n_0}{\sqrt{2n_0 n_+}} \cos \phi_+ + \frac{2n_- - n_0}{\sqrt{2n_0 n_-}} \cos \phi_- \right], \\ \dot{m} &= p\sqrt{2n_0}[-\sqrt{n_+} \sin \phi_+ + \sqrt{n_-} \sin \phi_-], \\ \dot{\eta} &= -2m - p\sqrt{\frac{n_0}{2}} \left[\frac{\cos \phi_+}{\sqrt{n_+}} - \frac{\cos \phi_-}{\sqrt{n_-}} \right], \end{aligned} \quad (3)$$

where ϕ_\pm and n_\pm are functions of n_0 , m , θ , and η . The respective classical trajectories are obtained through numerical integration of these equations.

Quantum scars and regular eigenstates.—The presence of a clear classical limit in our model allows one to visualize ergodicity breaking directly in phase space using the Husimi-Q distribution $Q_n(\zeta) = |\langle \zeta | \psi_n \rangle|^2$ of each quantum eigenstate $|\psi_n\rangle$, obtained through exact diagonalization of Eq. (2) for $N = 200$ atoms. As it will be argued later, it is convenient for visualization purposes to focus on the (n_0, θ) plane, in which we define a projection function

$$\mathcal{P}_n(n_0, \theta) = \frac{1}{d(n_0, \theta)} \iint dmd\eta Q_n(n_0, \theta, m, \eta), \quad (4)$$

where $d(n_0, \theta) = \iint dmd\eta \delta(E_n - \langle \zeta | \hat{H} | \zeta \rangle)$ is the density of states at energy E_n in the classical phase space.

We present \mathcal{P}_n for some characteristic eigenstates in Figs. 1(b)–1(d). Remarkably, we find that most eigenstates exhibit a structure in phase space [46–48], even those [panels (c),(d)] with large entropy [see panel (a)]. Indeed, the patterns observed in $\mathcal{P}_n(n_0, \theta)$ can be associated with periodic trajectories of the classical equations of motion, Eq. (3). These lead to a mixed phase space with both regular and chaotic regions, as can be seen from an analysis based on Poincaré sections and Lyapunov exponents [Fig. 2(a)]. Because of energy conservation, the motion is constrained to a three-dimensional manifold, and a 2D Poincaré section of equal-energy trajectories is thus obtained by fixing one variable. We choose to display (n_0, θ) for those times t at which $m(t) = m(0)$. For each point on the Poincaré section, we extract the Lyapunov exponent λ from the monodromy matrix [58], and imprint it in the marker’s color. For small n_0 we observe stable regular trajectories ($\lambda = 0$). The motion becomes chaotic ($\lambda > 0$) for larger n_0 . Interestingly, it is seen from Eq. (3) that a trajectory starting on the 2D plane defined by $m = 0$ and $\eta = 0, 2\pi$ remains on the plane. Evolving with Hamiltonian dynamics in 2D, these trajectories are periodic. However, some of these in-plane periodic orbits are unstable to out-of-plane perturbations, which is witnessed

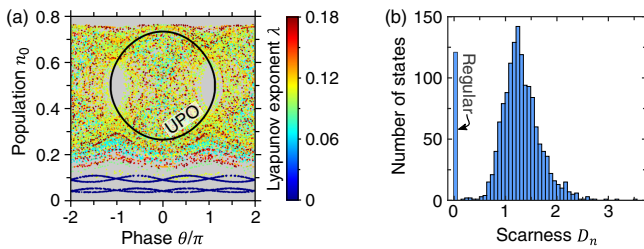


FIG. 2. (a) Poincaré section of the classical equations of motion Eq. (3) at energy $E/N = 0.24$, showing a mixed phase space. The colors represent the Lyapunov exponent λ of trajectories in phase space. The UPO at the same energy is represented by a solid black line ($\lambda_{\text{UPO}} = 0.12$). The dark blue dots at $n_0 \ll 1$ correspond to stable periodic orbits ($\lambda \approx 0$). The density of states vanishes in the gray background. (b) Distribution of the scarness D_n for 10^3 eigenstates at energy $E = 0.24 N$.

by a positive Lyapunov exponent $\lambda > 0$. These UPOs are responsible for scarring the eigenstates; see Fig. 1(c).

We emphasize that scarring is very different from the correspondence between regular states and *stable* (quasi) periodic orbits. This can be understood from semiclassical arguments such as the Einstein-Brillouin-Keller quantization method for integrable models. This method applies when a *volume* in phase space is regular, but cannot explain the scarring by UPOs that constitute a measure zero set [25,70].

To quantify the scarring of the eigenstates $|\psi_n\rangle$, we define a “scarness” figure of merit (see also [48,71–73]),

$$D_n = \frac{\int_{\text{UPO}} d\zeta |\langle \psi_n | \zeta \rangle|^2}{\int_{\text{UPO}} d\zeta |\langle \psi_e | \zeta \rangle|^2}. \quad (5)$$

Here, the numerator (denominator) quantifies the overlap of the UPO with an eigenstate $|\psi_n\rangle$ (ergodic state $|\psi_e\rangle$) at energy E_n . The ergodic state $|\psi_e\rangle$ is built as a superposition of 10^4 coherent states taken along a randomly picked classical chaotic trajectory at energy E_n . We thus expect $D_n \approx 1$ if $|\psi_n\rangle$ is not scarred, $D_n > 1$ if it is scarred by the considered UPO, and $D_n < 1$ if $|\psi_n\rangle$ is scarred by another UPO or if it is a regular state. In Fig. 2(b), we show the histogram of D_n in the middle of the energy spectrum. The peak at $D_n \approx 0$ is due to the regular states, which fill a region of phase space not explored by the UPO. Except for this, the distribution of D_n is biased toward values $D_n > 1$ (excluding the regular states, the mean value of D_n is ≈ 1.3), suggesting that most eigenstates are scarred by the UPOs that we have previously identified. Finally, note that by adding the term $\propto \delta_z \hat{S}_z$ to the Hamiltonian Eq. (2) (experimentally realized by detuning the frequency of the rotating fields), the $m = \eta = 0$ plane no longer hosts UPOs, and consequently, the Husimi distributions of the eigenstates do not show any scars.

QMBS feature low entropy and violate ETH, two key properties that we now investigate for our scarred and regular states. Unlike QMBS, we could not find an entropic measure that is significantly affected by the scarring. First, we inspect the von Neumann entropy $\mathcal{S}_n^{(1)} = -\text{Tr}[\rho_n^{(1)} \ln \rho_n^{(1)}]$ of the one-body density matrix $[\rho_n^{(1)}]_{jk} = \langle \psi_n | \hat{a}_j^\dagger \hat{a}_k | \psi_n \rangle$, which quantifies the entanglement between one atom and the rest of the ensemble [74]. This entropy is large for all scarred states, c.f., Fig. 1, with no appreciable dependence on D_n . We have also checked the mode entanglement entropy [75], which is similarly large, while slightly anticorrelated with D_n (see SM [58]).

Let us now focus on the thermalization properties and energy level statistics. Figure 3(a) shows the expectation values of $\hat{n}_0 = \hat{N}_0/N$ for each eigenstate $|\psi_n\rangle$, where $\langle \hat{n}_0 \rangle$ is a commonly measured quantity in spinor experiments [55,56,76] (similar behaviors are found for other few-body observables). Across the range $0.22 < E/N < 0.32$, there

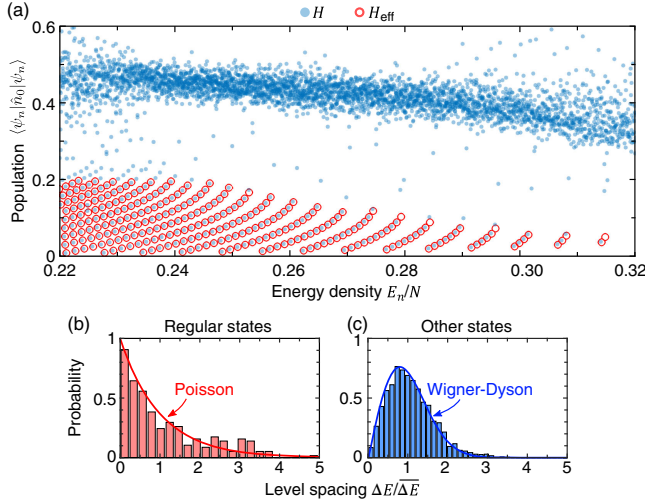


FIG. 3. (a) Eigenstate expectation values $\langle \hat{n}_0 \rangle$, showing a narrow branch of thermal states with small fluctuations of $\langle \hat{n}_0 \rangle$, in agreement with ETH, and towers of regular states violating ETH. The red circles are obtained from a numerical diagonalization of the effective Hamiltonian Eq. (6). Level spacing statistics for the regular (b) and thermal (c) states. The solid lines depict the Poisson and the Wigner-Dyson distributions, respectively.

is a band of thermal states where $\langle \hat{n}_0 \rangle$ is a smooth function of energy, in agreement with the ETH [33] (see SM [58] for details). By contrast, $\langle \hat{n}_0 \rangle$ is organized in towers for the regular states and violates the ETH [58]. Consistently, in Figs. 3(b) and 3(c) we demonstrate that the level spacing statistics is close to the Poisson and Wigner-Dyson distributions for thermal and regular states, respectively.

These findings suggest that the regular states can be obtained from an underlying integrable model. Indeed, we are able to unravel it with the following reasoning: when there is a significant imbalance $N_+ \gg N_-$, we expect bosonic amplification of the mixing between $m = 0$ and $m = +1$, leaving $m = -1$ as a background mode. In this case \hat{W}_- can be neglected, the conservation of \hat{N}_- is restored, and the eigenstates are Fock states for the $m = -1$ mode. We can thus replace the operator \hat{N}_- by its eigenvalue N_- , and obtain the following integrable Hamiltonian for the remaining $m = 0, +1$ modes:

$$\hat{H}_{\text{eff}}(N_-) = -\frac{\hat{N}_0^2}{2N} + \frac{2N_-}{N} \hat{N}_0 + p\hat{W}_+ + C, \quad (6)$$

where C is a constant [58]. For a fixed N_- we diagonalize numerically $\hat{H}_{\text{eff}}(N_-)$, and find eigenstate expectation values that match remarkably well those of a given tower. Considering a wide range of N_- we are able to reconstruct all the towers seen in Fig. 3(a). Note that, to mitigate finite size effects, we diagonalize the Hamiltonian of Eq. (6) for $N = 2000$ (instead of $N = 200$), and examine one eigenstate in every ten (details in SM [58]). There are $\propto N$ towers

of $\propto N$ states, yielding a total number of regular states $\propto N^2$, which constitutes a finite fraction of the Hilbert space (with dimension $\propto N^2$), even in the thermodynamic limit.

In the limit $N_0 \ll N_+$, Eq. (6) can be linearized and diagonalized via a Bogoliubov transformation. Hence the regular states can be constructed analytically from a set of two spectrum generating algebras, a common tool to construct QMBS [17–19] (although these algebras here are approximate and only capture some regular states, see SM [58]). Within this approximation, the towers of regular eigenstates can be seen as independent harmonic oscillators, explaining the Poisson energy level statistics. Finally, note that another set of regular states is obtained upon inverting the role of the $m = \pm 1$ modes, leading to nearly degenerate doublets of regular states.

Dynamics.—We now investigate the dynamics of the system; see Fig. 4. We consider three initial states at the energy $E = 0.24 N$: (i) a coherent state $|\zeta_c\rangle$ with $n_0 = (1 + \sqrt{1 - 4E/N})/2$, $\eta = \pi$, and $m = \theta = 0$, such that ζ_c overlaps with the chaotic region of the phase space; (ii) a coherent state $|\zeta_s\rangle$ with $n_0 = (1 + \sqrt{1 - 4E/N})/2$, $m = \eta = 0$, and $\theta = \pi$, such that ζ_s lies on the UPO; and (iii) a Fock state $|\psi_{\text{reg}}\rangle$ with $N_0 = 0$ and $N_+ - N_- = \sqrt{2NE}$, chosen to have a large overlap with one tower of regular states. We focus on the observable $\langle \hat{n}_0 \rangle$, though we observe similar behavior for other few-body observables.

Regular states display long-lived oscillations in the time evolution of both $\langle \hat{n}_0 \rangle$ and the state fidelity $\mathcal{F}(t) = |\langle \psi(0) | \psi(t) \rangle|^2$, independently of the system size; see Figs. 4(a) and 4(b), respectively. On the other hand, when the system is initiated at the two coherent states $|\zeta_c\rangle$ and $|\zeta_s\rangle$ [57], which overlap with eigenstates satisfying ETH, \hat{n}_0 rapidly thermalizes to the microcanonical ensemble prediction (excluding the regular states). The role of scarring

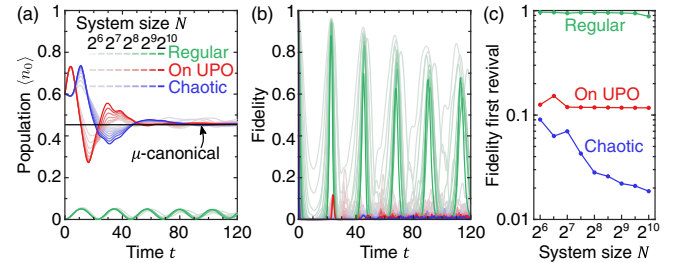


FIG. 4. Time evolution of (a) $\langle \hat{n}_0 \rangle$ and (b) the fidelity for an initial Fock state overlapping with regular states (green lines), a coherent state initiated on a UPO (red lines) and a coherent state in the chaotic sea (blue lines). The line intensity denotes increasing atom number (from 64 to $N = 1024$). In (a), the solid black line is the microcanonical ensemble prediction with an energy window that excludes the regular states, and it is identical for all initial states that are at the same energy $E = 0.24 N$. In (c), we show the fidelity achieved at the first revival as a function of the atom number.

becomes evident at the level of the fidelity $\mathcal{F}(t)$ [Fig. 4(b)]: its first revival is stable in the $N \gg 1$ limit for the initial state $|\zeta_s\rangle$, whereas it vanishes for the initial state $|\zeta_c\rangle$. This can be better appreciated from the scaling analysis in Fig. 4(c).

Discussion and outlook.—We have studied a chaotic spinor condensate in which a semiclassical limit allows one to unambiguously discern coexisting quantum scars and regular eigenstates. We recover the properties of chaotic many-body systems with ETH-obeying and high-entropy eigenstates, and Wigner-Dyson energy spacing distribution. Remarkably, these features arise despite the fact that most eigenstates are scarred [48], instead of random as expected for a chaotic system [5]. These results also highlight the difference between quantum scars [27] and QMBS, which are often defined as nonthermal eigenstates [18,19,24]—a definition that in our system would point toward regular states. An interesting open question remains regarding the fate of regular and scar states upon breaking the all-to-all nature of the model, e.g., when loading the spinor condensate in an optical lattice [77].

Our model’s main ingredients are readily available in state-of-the-art experimental setups, which is an exciting prospect given the scarcity of experimental observations of quantum scars [26,78] in a many-body setting. It could provide an ideal test bed to investigate the relation between scarring and decoherence in a physical system with a weak coupling to the environment [22].

We thank Eric J. Heller, Joonas Keski-Rahkonen, Francisco L. Machado, Hannes Pichler, Saúl Pilatowsky-Cameo, and H.R. Sadeghpour for helpful comments and discussions. B.E. is supported by an ETH Zurich Postdoctoral Fellowship. A.P. is supported by the AFOSR MURI program (Grant No. FA9550-21-1-0069). C.B.D. and S.I.M. acknowledge financial support from the NSF through a grant for ITAMP (Grant No. 2116679) at Harvard University.

*Corresponding author: bevrard@phys.ethz.ch

†Corresponding author: ceren.dag@cfa.harvard.edu

- [1] J. M. Deutsch, *Phys. Rev. A* **43**, 2046 (1991).
- [2] M. Srednicki, *Phys. Rev. E* **50**, 888 (1994).
- [3] R. V. Jensen and R. Shankar, *Phys. Rev. Lett.* **54**, 1879 (1985).
- [4] M. Rigol, V. Dunjko, and M. Olshanii, *Nature (London)* **452**, 854 (2008).
- [5] L. D’Alessio, Y. Kafri, A. Polkovnikov, and M. Rigol, *Adv. Phys.* **65**, 239 (2016).
- [6] H. Kim, T. N. Ikeda, and D. A. Huse, *Phys. Rev. E* **90**, 052105 (2014).
- [7] T. Kinoshita, T. Wenger, and D. S. Weiss, *Nature (London)* **440**, 900 (2006).
- [8] M. Rigol, V. Dunjko, V. Yurovsky, and M. Olshanii, *Phys. Rev. Lett.* **98**, 050405 (2007).
- [9] M. Rigol, *Phys. Rev. Lett.* **103**, 100403 (2009).
- [10] P. Sala, T. Rakovszky, R. Verresen, M. Knap, and F. Pollmann, *Phys. Rev. X* **10**, 011047 (2020).
- [11] V. Khemani, M. Hermele, and R. Nandkishore, *Phys. Rev. B* **101**, 174204 (2020).
- [12] D. M. Basko, I. L. Aleiner, and B. L. Altshuler, *Ann. Phys. (Amsterdam)* **321**, 1126 (2006).
- [13] M. Schreiber, S. S. Hodgman, P. Bordia, H. P. Lüschen, M. H. Fischer, R. Vosk, E. Altman, U. Schneider, and I. Bloch, *Science* **349**, 842 (2015).
- [14] R. Nandkishore and D. A. Huse, *Annu. Rev. Condens. Matter Phys.* **6**, 15 (2015).
- [15] N. Shiraishi and T. Mori, *Phys. Rev. Lett.* **119**, 030601 (2017).
- [16] H. Bernien, S. Schwartz, A. Keesling, H. Levine, A. Omran, H. Pichler, S. Choi, A. S. Zibrov, M. Endres, M. Greiner *et al.*, *Nature (London)* **551**, 579 (2017).
- [17] C. J. Turner, A. A. Michailidis, D. A. Abanin, M. Serbyn, and Z. Papić, *Nat. Phys.* **14**, 745 (2018).
- [18] S. Moudgalya, S. Rachel, B. A. Bernevig, and N. Regnault, *Phys. Rev. B* **98**, 235155 (2018).
- [19] M. Serbyn, D. A. Abanin, and Z. Papić, *Nat. Phys.* **17**, 675 (2021).
- [20] G.-X. Su, H. Sun, A. Hudomal, J.-Y. Desaulles, Z.-Y. Zhou, B. Yang, J. C. Halimeh, Z.-S. Yuan, Z. Papić, and J.-W. Pan, *Phys. Rev. Res.* **5**, 023010 (2023).
- [21] P. Zhang, H. Dong, Y. Gao, L. Zhao, J. Hao, J.-Y. Desaulles, Q. Guo, J. Chen, J. Deng, B. Liu *et al.*, *Nat. Phys.* **19**, 120 (2023).
- [22] B. Buča, J. Tindall, and D. Jaksch, *Nat. Commun.* **10**, 1730 (2019).
- [23] M. Schecter and T. Iadecola, *Phys. Rev. Lett.* **123**, 147201 (2019).
- [24] S. Moudgalya, B. A. Bernevig, and N. Regnault, *Rep. Prog. Phys.* (2022).
- [25] E. J. Heller, *The Semiclassical Way to Dynamics and Spectroscopy* (Princeton University Press, Princeton, NJ, 2018).
- [26] J. Stein and H.-J. Stöckmann, *Phys. Rev. Lett.* **68**, 2867 (1992).
- [27] E. J. Heller, *Phys. Rev. Lett.* **53**, 1515 (1984).
- [28] W. W. Ho, S. Choi, H. Pichler, and M. D. Lukin, *Phys. Rev. Lett.* **122**, 040603 (2019).
- [29] A. A. Michailidis, C. J. Turner, Z. Papić, D. A. Abanin, and M. Serbyn, *Phys. Rev. X* **10**, 011055 (2020).
- [30] C. J. Turner, J.-Y. Desaulles, K. Bull, and Z. Papić, *Phys. Rev. X* **11**, 021021 (2021).
- [31] E. Boukobza, M. G. Moore, D. Cohen, and A. Vardi, *Phys. Rev. Lett.* **104**, 240402 (2010).
- [32] T. Mori, *Phys. Rev. E* **96**, 012134 (2017).
- [33] C. B. Dağ, S.-T. Wang, and L.-M. Duan, *Phys. Rev. A* **97**, 023603 (2018).
- [34] S. Sinha and S. Sinha, *Phys. Rev. Lett.* **125**, 134101 (2020).
- [35] M. Rautenberg and M. Gärtner, *Phys. Rev. A* **101**, 053604 (2020).
- [36] Q. Hummel, K. Richter, and P. Schlagheck, *Phys. Rev. Lett.* **130**, 250402 (2023).
- [37] Karin Wittmann W., E. R. Castro, A. Foerster, and L. F. Santos, *Phys. Rev. E* **105**, 034204 (2022).
- [38] S. Sinha, S. Ray, and S. Sinha, arXiv:2309.15527.

- [39] Y. Kawaguchi and M. Ueda, *Phys. Rep.* **520**, 253 (2012).
- [40] D. M. Stamper-Kurn and M. Ueda, *Rev. Mod. Phys.* **85**, 1191 (2013).
- [41] M.-S. Chang, Q. Qin, W. Zhang, L. You, and M. S. Chapman, *Nat. Phys.* **1**, 111 (2005).
- [42] L. E. Sadler, J. M. Higbie, S. R. Leslie, M. Vengalattore, and D. M. Stamper-Kurn, *Nature (London)* **443**, 312 (2006).
- [43] M. Prüfer, P. Kunkel, H. Strobel, S. Lannig, D. Linnemann, C.-M. Schmied, J. Berges, T. Gasenzer, and M. K. Oberthaler, *Nature (London)* **563**, 217 (2018).
- [44] S. Huh, K. Mukherjee, K. Kwon, J. Seo, S. I. Mistakidis, H. R. Sadeghpour, and J.-y. Choi, *arXiv:2303.05230*.
- [45] J. Tomkovič, W. Muessel, H. Strobel, S. Löck, P. Schlagheck, R. Ketzmerick, and M. K. Oberthaler, *Phys. Rev. A* **95**, 011602(R) (2017).
- [46] J. Keski-Rahkonen, P. J. J. Luukko, S. Åberg, and E. Räsänen, *J. Phys. Condens. Matter* **31**, 105301 (2019).
- [47] D. Mondal, S. Sinha, and S. Sinha, *Phys. Rev. E* **102**, 020101(R) (2020).
- [48] S. Pilatowsky-Cameo, D. Villaseñor, M. A. Bastarrachea-Magnani, S. Lerma-Hernández, L. F. Santos, and J. G. Hirsch, *Nat. Commun.* **12**, 852 (2021).
- [49] L. P. Pitaevskii and A. Rosch, *Phys. Rev. A* **55**, R853 (1997).
- [50] C. N. Yang, *Phys. Rev. Lett.* **63**, 2144 (1989).
- [51] T. Ohmi and K. Machida, *J. Phys. Soc. Jpn.* **67**, 1822 (1998).
- [52] C. K. Law, H. Pu, and N. P. Bigelow, *Phys. Rev. Lett.* **81**, 5257 (1998).
- [53] T.-L. Ho, *Phys. Rev. Lett.* **81**, 742 (1998).
- [54] S. Yi, Ö. Müstecaplıoğlu, C.-P. Sun, and L. You, *Phys. Rev. A* **66**, 011601(R) (2002).
- [55] H.-X. Yang, T. Tian, Y.-B. Yang, L.-Y. Qiu, H.-Y. Liang, A.-J. Chu, C. B. Dağ, Y. Xu, Y. Liu, and L.-M. Duan, *Phys. Rev. A* **100**, 013622 (2019).
- [56] B. Evrard, A. Qu, J. Dalibard, and F. Gerbier, *Phys. Rev. Lett.* **126**, 063401 (2021).
- [57] B. Evrard, A. Qu, J. Dalibard, and F. Gerbier, *Phys. Rev. A* **103**, L031302 (2021).
- [58] See Supplemental Material at <http://link.aps.org/supplemental/10.1103/PhysRevLett.132.020401> for the details on experimental proposal and the model, eigenstate thermalization hypothesis calculations, approximate spectrum generating algebras for the regular eigenstates, and the orbit analysis in the phase space, which includes Refs. [59–68].
- [59] S. I. Mistakidis, A. G. Volosniev, R. E. Barfknecht, T. Fogarty, T. Busch, A. Foerster, P. Schmelcher, and N. T. Zinner, *Phys. Rep.* **1042**, 1 (2023).
- [60] K. M. Mittal, S. I. Mistakidis, P. G. Kevrekidis, and P. Schmelcher, *Phys. Rev. A* **102**, 013302 (2020).
- [61] E. M. Bookjans, A. Vinit, and C. Raman, *Phys. Rev. Lett.* **107**, 195306 (2011).
- [62] A. Farolfi, D. Trypogeorgos, G. Colzi, E. Fava, G. Lamporesi, and G. Ferrari, *Rev. Sci. Instrum.* **90**, 115114 (2019).
- [63] M. Srednicki, *J. Phys. A* **29**, L75 (1996).
- [64] M. Srednicki, *J. Phys. A* **32**, 1163 (1999).
- [65] R. Gati and M. K. Oberthaler, *J. Phys. B* **40**, R61 (2007).
- [66] S. Moudgalya, N. Regnault, and B. A. Bernevig, *Phys. Rev. B* **102**, 085140 (2020).
- [67] P. Gaspard, *Chaos, Scattering and Statistical Mechanics*, Cambridge Nonlinear Science Series (Cambridge University Press, Cambridge, England, 1998), 10.1017/CBO9780511628856.
- [68] T. Parker and L. Chua, *Practical Numerical Algorithms for Chaotic Systems* (Springer, New York, 2012).
- [69] The ferromagnetic case of $c_1 < 0$, found, e.g., for ^{87}Rb or ^7Li atoms, is analogous: upon changing the sign of p (which can be achieved with a unitary transformation), one implements $\hat{H} \rightarrow -\hat{H}$ that flips the sign of the eigenvalues while not affecting the eigenstates. Hence the findings and conclusions of this work remain valid.
- [70] M. V. Berry, *J. Phys. A* **10**, 2083 (1977).
- [71] P. J. J. Luukko, B. Drury, A. Klales, L. Kaplan, E. J. Heller, and E. Räsänen, *Sci. Rep.* **6**, 37656 (2016).
- [72] J. Keski-Rahkonen, A. Ruhanen, E. J. Heller, and E. Räsänen, *Phys. Rev. Lett.* **123**, 214101 (2019).
- [73] S. Pilatowsky-Cameo, D. Villaseñor, M. A. Bastarrachea-Magnani, S. Lerma-Hernández, L. F. Santos, and J. G. Hirsch, *New J. Phys.* **23**, 033045 (2021).
- [74] B. Evrard, A. Qu, J. Dalibard, and F. Gerbier, *Science* **373**, 1340 (2021).
- [75] V. Vedral, *Central Eur. J. Phys.* **1**, 289 (2003).
- [76] Z. Chen, T. Tang, J. Austin, Z. Shaw, L. Zhao, and Y. Liu, *Phys. Rev. Lett.* **123**, 113002 (2019).
- [77] H. Zhao, J. Vovrosh, F. Mintert, and J. Knolle, *Phys. Rev. Lett.* **124**, 160604 (2020).
- [78] P. B. Wilkinson, T. M. Fromhold, L. Eaves, F. W. Sheard, N. Miura, and T. Takamasu, *Nature (London)* **380**, 608 (1996).